

The Thousand-Pulsar-Array programme on MeerKAT XI: Application of the rotating vector model

S. Johnston^{1*}, M. Kramer², A. Karastergiou^{3,4}, M. J. Keith⁵, L. S. Oswald^{3,6},
A. Parthasarathy², P. Weltevrede⁵

¹Australia Telescope National Facility, CSIRO Space and Astronomy, PO Box 76, Epping NSW 1710, Australia

²Max-Planck-Institut für Radioastronomie, Auf dem Hügel 69, D-53121 Bonn, Germany

³Department of Astrophysics, University of Oxford, Denys Wilkinson Building, Keble Road, Oxford OX1 3RH, UK

⁴Department of Physics and Electronics, Rhodes University, PO Box 94, Grahamstown 6140, South Africa

⁵Jodrell Bank Centre for Astrophysics, Department of Physics and Astronomy, University of Manchester, Manchester M13 9PL, UK

⁶Magdalen College, University of Oxford, Oxford OX1 4AU, UK

Last updated; in original form

ABSTRACT

In spite of the rich phenomenology of the polarization properties of radio pulsars, the rotating vector model (RVM) created 50 years ago remains the best method to determine the beam geometry of a pulsar. We apply the RVM to a sample of 854 radio pulsars observed with the MeerKAT telescope in order to draw conclusions about the population of pulsars as a whole. The main results are that (i) the geometrical interpretation of the position angle traverse is valid in the majority of the population, (ii) the pulsars for which the RVM fails tend to have a high fraction of circular polarization compared to linear polarization, (iii) emission heights obtained through both geometrical and relativistic methods show that the majority of pulsars must have emission heights less than 1000 km independent of spin period, (iv) orthogonal mode jumps are seen in the position angle traverse in about one third of the population. All these results are weakly dependent on the pulsar spin-down energy.

Key words: pulsars:general

1 INTRODUCTION

Arguably the most important characteristics of a pulsar are its spin period, P , its spin-down energy loss-rate, \dot{E} , and its geometry. The offset between the magnetic and rotation axes (denoted by α) and the traverse of the observer's line-of-sight determines whether or not a pulsar is visible and the shape and polarization of its pulse profile. Furthermore, the birth distribution of α and its evolution with time are critical to understanding the population of pulsars as a whole and the formation process of neutron stars. P and \dot{E} are trivial to measure, and values exist for some 3000 pulsars. The geometrical angles are much harder to determine and unambiguous values exist for at best a few tens of pulsars.

In the rotating vector model (RVM) of Radhakrishnan & Cooke (1969), the radio radiation is beamed along the field lines and the plane of polarization is determined by the orientation of the magnetic field as it sweeps past the line of sight. The position angle (PA) as a function of pulse longitude, ϕ , can be expressed as

$$\text{PA} = \text{PA}_0 + \arctan\left(\frac{\sin\alpha \sin(\phi - \phi_0)}{\sin\zeta \cos\alpha - \cos\zeta \sin\alpha \cos(\phi - \phi_0)}\right) \quad (1)$$

Here, $\zeta = \alpha + \beta$ with β being the angle of closest approach of the line of sight to the magnetic axis. ϕ_0 is the pulse longitude at which

the PA is PA_0 , which also corresponds to the PA of the rotation axis projected onto the plane of the sky.

The textbook picture of radio pulsars has emission arising from close to the surface, at a height h_{em} , and is bounded by the open field lines. The half-opening angle of the emission cone, ρ , is then given by

$$\rho = \sqrt{\frac{9 \pi h_{\text{em}}}{2 P c}} \quad (2)$$

(Rankin 1990) with P the spin period and c the speed of light. In turn, the observed pulse width is related to ρ via the geometry and can be expressed (Gil et al. 1984) as

$$\cos\rho = \cos\alpha \cos\zeta + \sin\alpha \sin\zeta \cos(W_{10}/2) \quad (3)$$

where W_{10} is the pulse width measured at 10% of the peak flux (e.g. Posselt et al. 2021). Furthermore, relativistic effects are important due to the rapid rotation of the magnetosphere as initially discussed in Blaskiewicz et al. (1991). They showed that the location of the inflection point of the PA swing is delayed with respect to the centre of the pulse profile by an amount given by

$$\Delta\phi = \frac{8 \pi h_{\text{em}}}{P c} \quad (4)$$

For a pulsar with $P = 0.25$ s and $h_{\text{em}} = 300$ km, $\rho \approx 14^\circ$ and for α not too low then $W_{10} \approx 28^\circ$ and $\Delta\phi \approx 6^\circ$. Alternatively, measurements of $\Delta\phi$ and/or W_{10} can help constrain h_{em} . This approach, and its pitfalls, are outlined in e.g. Weltevrede & Johnston (2008b). It should

* Email: simon.johnston@csiro.au

Table 1. Results of the RVM fitting by class. Column 2 lists the number in each class. Columns 3 and 4 indicate the sign of β . In columns 5 and 6 we denote as V_h those pulsars for which $|V| > L$ in 5 bins or more across the profile and V_l those pulsars for which this is not the case. The final three columns indicate the offset between the location of ϕ_0 and the profile midpoint. See text for details.

Class	Number	$\beta < 0$	$\beta > 0$	V_h	V_l	$\Delta\phi < -1^\circ$	$ \Delta\phi < 1^\circ$	$\Delta\phi > 1^\circ$
RVM	431	224	207	72	359	79	86	266
flat	71	43	28	6	65			
non RVM	352			210	142			
Total	854							

be noted that the standard picture of a hollow cone of emission (Rankin 1983, 1990; Lyne & Manchester 1988; Mitra & Rankin 2002) has come under close scrutiny, and an alternative model which invokes ‘flux tubes’ or ‘fan-beams’ is equally good at reproducing the observed phenomenology (Wang et al. 2014; Dyks & Rudak 2015; Dyks 2017; Oswald et al. 2019). From a theoretical perspective, Equation 2 assumes a circular polar cap and no distortion of the magnetosphere, both of which are questionable (e.g. Gangadhara 2004; Yuen & Melrose 2014; Lockhart et al. 2019).

In spite of the simplicity of the geometrical argument for the PA traverse, many open questions remain. In about half of all pulsars, the PA traverse does not conform to the RVM and reasons for this must be sought. The main explanation comes from propagation through the magnetosphere, including refraction of the modes (Weltevrede et al. 2003; Fussell & Luo 2004; Beskin & Philippov 2012), coherent mode mixing (Dyks 2019) and generalised Faraday rotation (Kennett & Melrose 1998; Ilie et al. 2019). In addition, it is likely that the various components of the pulse profile arise at different emission heights, with outer components originating from higher in the magnetosphere (Yuen & Melrose 2014; Johnston & Kramer 2019; Desvignes et al. 2019) where sweepback of the magnetic field lines might be important (Craig & Romani 2012). Finally, the dipolar field may be offset from the star’s centre and/or quadrupole or higher-order fields may be important (e.g. Pétri 2020). Furthermore, even for pulsars which show PA traverses compatible with the RVM, the narrow duty cycle of the pulse profile makes it difficult to determine a unique solution for α and β in the absence of further constraints (e.g. Rookyard et al. 2015b).

Although these objections may appear daunting, there is good reason to believe the validity of the RVM in many cases. In PSR J1906+0746 where the geometry changes with time due to precession of the beam, the RVM tracks the geometrical changes beautifully (Desvignes et al. 2019). Furthermore, in pulsars with interpulses, RVM fitting reflects the geometry of both the main and interpulse components (Weltevrede & Wright 2009; Johnston & Kramer 2019). In this paper we therefore attempt RVM fits for a sample of more than 1200 pulsars observed using the MeerKAT telescope. Section 2 briefly outlines the observations and the calibration procedure. Section 3 describes how the RVM fitting was performed and Section 4 details the results of the fitting. In Section 5 we present an analysis of the results and their implications for the population of pulsars as a whole.

2 OBSERVATIONS AND CALIBRATION

Observations were conducted as part of the Thousand Pulsar Array (TPA) program, itself part of the larger MeerTime project on the MeerKAT telescope. Details of the project as a whole and the observational setup can be found in Bailes et al. (2020) and Johnston et al. (2020). In brief, we used the observational band from 896 to

1671 MHz with 928 frequency channels. The data are folded into sub-integrations each of length 8 s for the duration of the observation and there are 1024 phase bins per pulse period. Polarization calibration is carried out using the procedures described in detail in Serylak et al. (2021). Flux calibration is carried out as described in Posselt et al. (2022). All these operations are performed by the processing pipeline MEERPIPE¹ which produces RFI-excised, polarization- and flux-calibrated output products in PSRFITS format (Hotan et al. 2004). A more complete description of the pipeline is reported in Parthasarathy et al. (2021). In this paper we use the same data set described in detail in Posselt et al. (2022).

3 RVM FITTING

The input data into the RVM fitter was a set of PAs and associated values of longitude, ϕ , taken from the set of pulsars presented in Posselt et al. (2022). The PAs were derived from Stokes Q and U, and were only determined when the linear polarization was more than 5σ significant. Error bars on the PAs were obtained from the value of the linear polarization compared to the noise using the procedure from Everett & Weisberg (2001). The peak of the profile was generally chosen as the zero point of longitude. RVM fitting was carried out using a least-squares procedure implemented in PYTHON. A total of 85 trials in α were used ranging from 5° to 175° . In β , 40 trials were used, initially between $\pm 20^\circ$, a range which could be refined on subsequent runs. For each α, β pair, the SCIPY routine LEAST_SQUARES was used to determine the values of ϕ_0 and PA_0 which minimized χ^2 and the minimum χ^2 was recorded. We note that PAs can only lie between -90° and $+90^\circ$ and hence the phase-wraps need to be taken into account. In addition, radio emission can appear in two orthogonal modes, and these so-called orthogonal mode transitions must also be built into the fitting routine.

In this work we use the so-called ‘observers convention’ which defines position angles as increasing counter-clockwise on the sky. This means that when the slope of the PA traverse is positive then the sign of β is negative. Also, when $\alpha < 90^\circ$ and $\beta > 0^\circ$ then we observe an **outer** line of sight (i.e. away from the spin axis and towards the equator). However, for $\alpha > 90^\circ$ and $\beta > 0^\circ$ we observe an **inner** line of sight (i.e. nearer to the spin axis). Therefore the sign of β alone does not reveal whether the sight line is inner or outer. For a detailed discussion see Everett & Weisberg (2001).

4 RVM FITTING RESULTS

The TPA census consists of 1267 pulsars and is fully described in Posselt et al. (2022). For the 21 interpulse pulsars in our sample, we

¹ <https://github.com/aparthas3112/meerpipe>

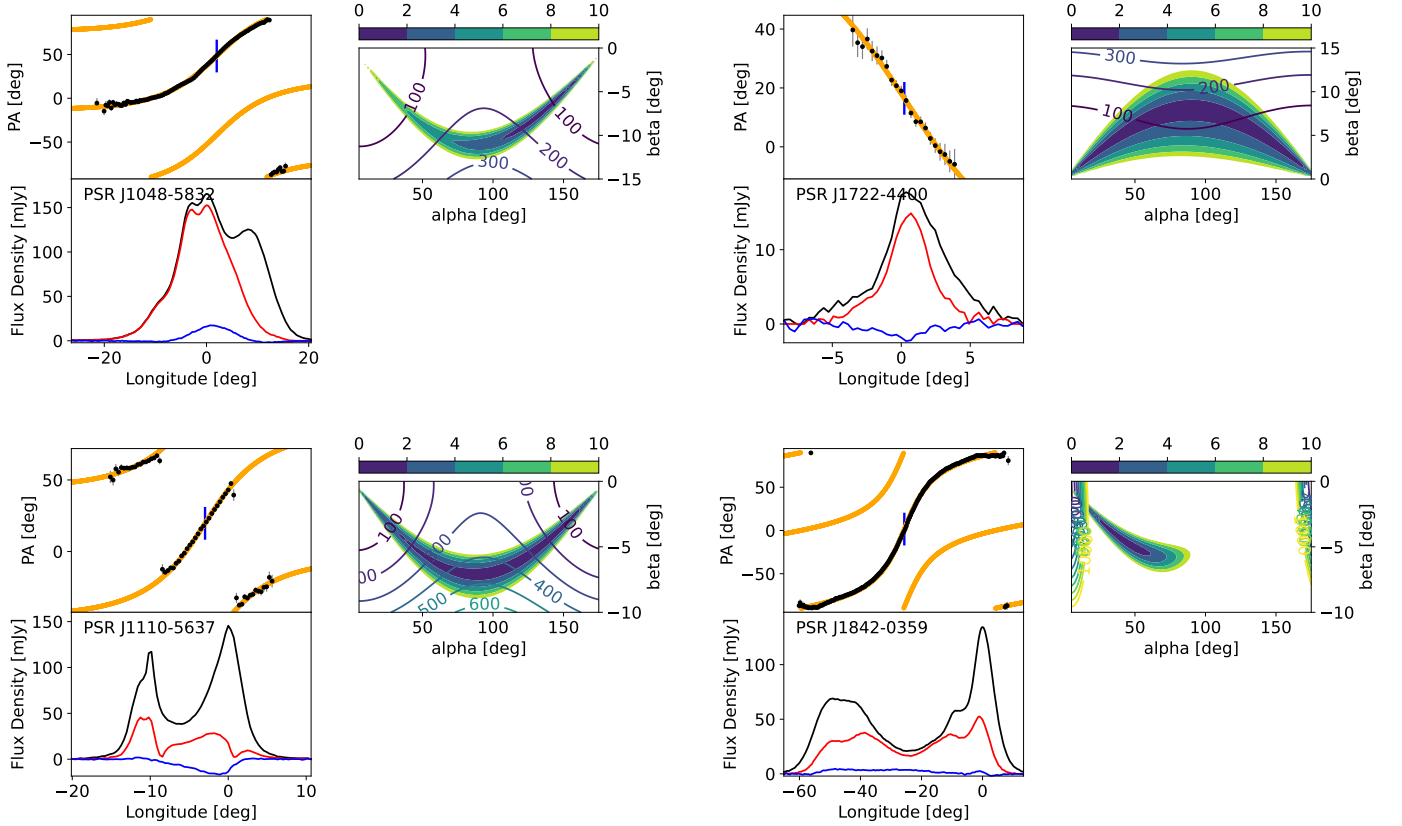


Figure 1. Examples of pulsars in the ‘RVM’ class for which the RVM fitting returns a low minimum value of χ^2 . The left-hand panels show the pulsar profile in Stokes I (black), linear polarization (red) and Stokes V (blue). The position angle of the linear polarization is shown in black. The best fit RVM is in orange, along with its 90° offset. The centre of the blue vertical line marks the inflection point. The right-hand panel shows the α – β plane, the image shows values of χ^2 from the fitting routine. Superposed are contours of height in km derived under the assumption that the beam is filled. The pulsars shown are PSRs J1048–5832, J1722–4400, J1110–5637 and J1842–0359.

performed independent fits on the main and interpulse components where sufficient PA points were available. Not all of the pulsars are amenable to RVM fitting. We required at least 10 PA points across the profile to proceed with the fit. This effectively removes pulsars for which the signal to noise ratio is low and pulsars which are bright but have very low level of linear polarization. In addition we removed pulsars which are scattered at our observing frequency as recorded in Oswald et al. (2021). Scattering has the effect of causing distortions in the PA swing due to the convolution of the Stokes Q and U profiles with an exponential function (Karastergiou 2009). These criteria led to a removal of 434 pulsars from the sample, listed in Table A4. This leaves a grand total of 854 RVM fit attempts.

There are three main classes of output from the fitter as detailed below, examples of which are given in Figures 1, 2 and 3. In Figure 1 the left-hand panels show the pulsar profile in total intensity, linear and circular polarization as a function of longitude, along with the position angle of the linear polarization. The right-hand panel shows an image of χ^2 values on the α – β plane. Lack of colour denotes $\chi^2 > 10$. In addition, contours of constant emission height are shown based on knowledge of W_{10} via equations 2 and 3. Meanwhile, Figures 2 and 3 show the profiles and the PA traverse only. The numbers in each class are shown in the second column of Table 1 and a visual representation of the results on the P – \dot{P} plane is shown in Figure 4.

A machine-readable ascii table with the full results is provided in the on-line material.

4.1 Class ‘RVM’

The pulsars in this class are those for which the RVM fitter returns a low value of reduced χ^2 , typically < 2 . Information on these pulsars is given in Table A1. In this class of pulsar, the PA is well-behaved over the entire profile, after orthogonal mode jumps are taken into account (see for example PSR J1110–5637 in Figure 1). The large majority of pulsars in this category show the classic ‘banana-shaped’ χ^2 contour plot on the α – β plane. This implies that α is unconstrained, the sign of β is determined, that $|\beta|$ has a maximum allowed value and that there exists a good χ^2 fit for a particular α, β pair.

The ‘banana’ can be thin either when the fit is excellent or when there is sufficient change of slope across the PA swing to sufficiently constrain β , as with PSR J1048–5832 in Figure 1. The ‘banana’ becomes thick for fits which are less good or when the slope has only changed marginally across the profile. An example is PSR J1722–4400 in Figure 1. In rare cases, the ‘banana’ can be resolved into a well-constrained part of the α – β plane. This happens only when the longitudinal extent of the profile is very wide or the pulsar has an interpulse. An example of the former is PSR J1842–0359 in Figure 1. It should also be noted that the values of PA_0 and ϕ_0 are (largely)

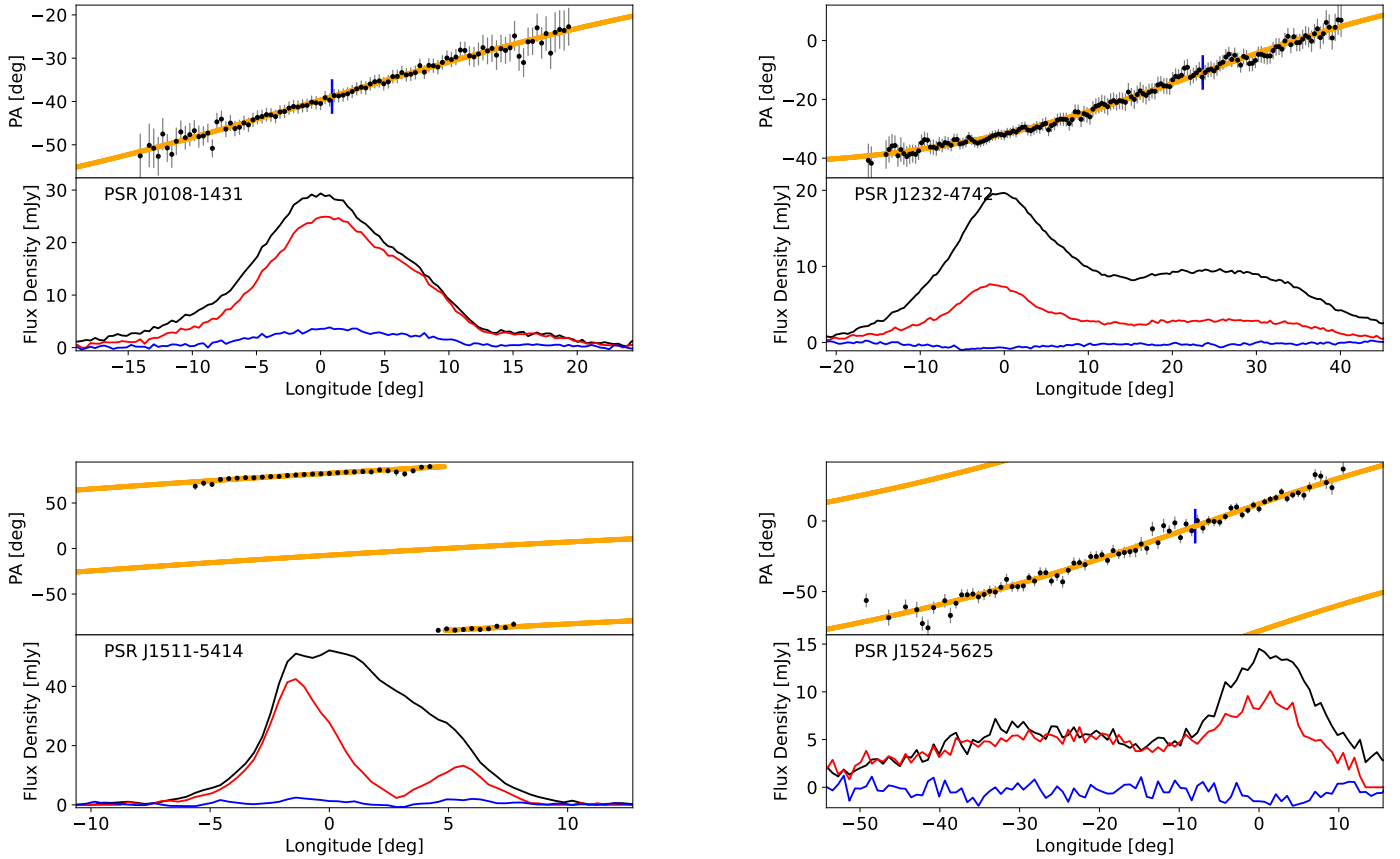


Figure 2. Examples of pulsars in the ‘flat’ class. PSRs J0108–1431, J1232–4742 and J1511–5414 are pulsars with low values of \dot{E} whereas PSR J1524–5625 has a high value of \dot{E} . All pulsars shown here have a PA slope which is less than 2 deg/deg.

independent of α and β . This is because the inflection point of the PA swing and hence the value of the PA at that location are relatively model-independent.

Finally, it can be seen that the lines of constant emission height make an almost orthogonal cut through the ‘banana’. If therefore the emission height is known, this provides a tight constraint on the α, β pair. Conversely if the geometry is well determined then the emission height can be derived.

4.2 Class ‘flat’

This class contains pulsars with a flat swing of PA across the profile, with a maximum swing of less than 2 degrees per degree and/or very little change in the overall slope as a function of longitude. For these pulsars, we cannot constrain either α or β , although the sign of β can at least be determined. The pulsars in this class are listed in Table A2, with four examples shown in Figure 2.

4.3 Class ‘non RVM’

Pulsars in this class contain PA swings which are forbidden by the RVM and are listed in Table A3. For example, some pulsars show several changes of direction in PA across the profile (see PSR J1625–4048 in Figure 3), while others show very large overall swings in PA (see PSR J2046–0421 in Figure 3). The fitting process returns high

values of χ^2 for these pulsars and no sensible constraints on the geometry can be obtained. However, for about 25% of the pulsars in this class, the PA swing looks broadly RVM-like, but with sufficient deviations to render the χ^2 high. An example is PSR J0846–3533 in Figure 3.

5 DISCUSSION

5.1 RVM versus non-RVM pulsars

Table 1 indicates that for the sample of 854 pulsars, some 60% of them have PA swings which appear RVM-like and 40% do not. What are the differences between these two classes? Figure 5 shows the distribution of \dot{E} for the entire sample, the RVM class, the flat class and non-RVM class. It can be seen that the RVM class has a distribution almost identical to that of the total sample whereas the flat class of pulsars is biased towards high \dot{E} and the non-RVM pulsars show a bias towards low values of \dot{E} . Indeed only 8 out of 77 pulsars with $\dot{E} > 10^{34.5}$ erg s $^{-1}$ are in the non-RVM class. In many ways this is not a surprise. Pulsars with high \dot{E} have previously been shown to have ‘simpler’ profiles with high degrees of linear polarization and unbroken PA swings (Johnston & Weisberg 2006; Rookyard et al. 2015b). This may arise because their emission heights are relatively high (Karastergiou & Johnston 2007) thus minimising the distortion of the polarization properties on the traverse through the

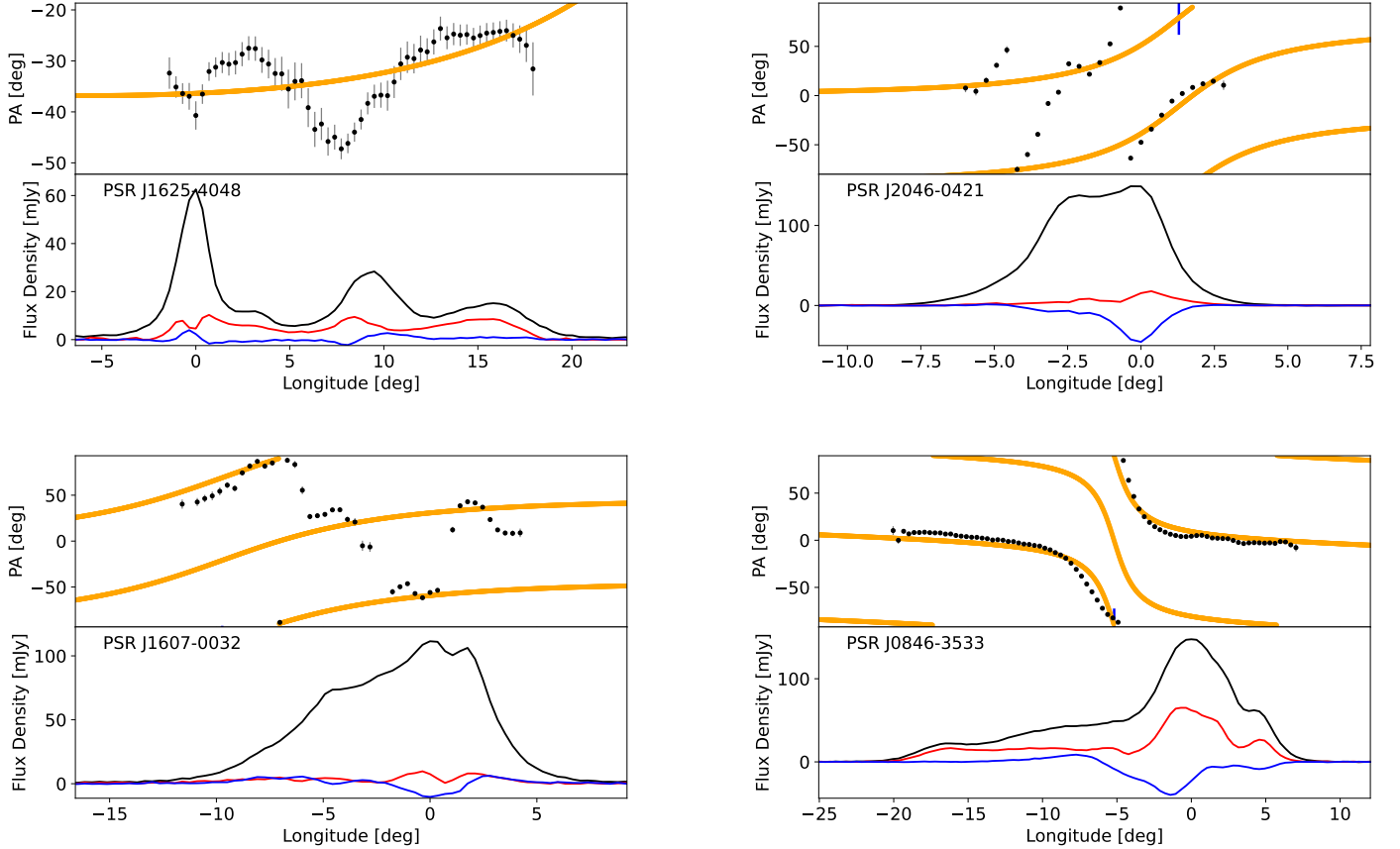


Figure 3. Examples of pulsars in the ‘non RVM’ class, for which the RVM fitting returns a high value of χ^2 . PSR J1625–4048 shows an example of a PA which changes direction several times across the profile. PSR J2046–0421 shows a very large PA swing across the profile. PSR J1607–0032 shows high levels of circular polarization compared to linear polarization. PSR J0846–3533 shows a PA swing with only minor deviations from an RVM-like curve.

magnetosphere. In contrast, the pulsars with low \dot{E} often have profiles which are a blend of multiple components (see Figure 3), possibly arising over a large range of emission heights, thereby distorting the PA swing (e.g. Craig & Romani 2012; Dyks 2017).

From visual inspection it is also apparent that pulsars in the non-RVM class have significantly more circular polarization (compared to linear polarization) than pulsars with RVM-like swings. To quantify this we determined how many pulsars have $|V| > L$ in more than 5 phase-bins across the profile, which we denote as V_h in Table 1. There are 288 such pulsars, 72% of which occur in the non-RVM class. Expressed another way, pulsars denoted as V_h occur 16% of the time in the RVM class and 59% in the non-RVM class. It therefore appears as a general, if not hard-and-fast rule, that distortions of the PA swing occur simultaneously with a high degree of circular polarization (see for example PSR J1607–0032 in Figure 3). Generation of circular polarization has long been a thorny problem in pulsar astronomy (Radhakrishnan & Rankin 1990; Kennett & Melrose 1998). In the simplest picture where two linearly polarized orthogonal modes interact incoherently, neither circular polarization nor distortion of the RVM curve can happen. Recently, Dyks (2019, 2020) pointed out that coherent addition of the modes with some (non-zero) phase lag not only generates circular polarization, but can also reproduce many of the peculiar PA traverses seen in single pulses. Motivated by this, Oswald et al. (2022) developed a framework for comparing the polarization properties of a large sample of pulsars to draw con-

clusions about the ratio of incoherent to coherent mixing (Oswald et al. In Prep.).

In the data presented here we also see manifestations of the same effect. In pulsars with an observed high fraction of linearly polarization, one mode dominates and any coherent mixing has a negligible effect on the PA swing. These tend to be the high \dot{E} pulsars. In pulsars with lower \dot{E} , the modes are more evenly matched in amplitude. As a result the linear polarization is low and coherent mixing can then produce significant circular polarization accompanied by distortions of the PA swing as observed. In a future paper we aim to take these ideas further by considering what mixing parameters are required to ‘fix’ the PA swing back to the geometrical RVM curve.

5.2 Flat PA swings

The pulsars with flat PA swings tend to be at high \dot{E} as shown in Figure 5. This class of pulsars was identified already in Johnston & Weisberg (2006). They have relatively short periods and hence large polar caps. This makes for a large beam and if α is low and the line of sight cuts the beam at high $|\beta|$ then the result is a wide profile with a flat PA swing (e.g. PSR J1524–5625, see Figure 2). Alternatively the emission height could be rather large, this would result in the PA swing leading the profile by a large amount (equation 4) meaning that we would miss the inflection point entirely.

However, there exists an interesting sub-category of pulsars with

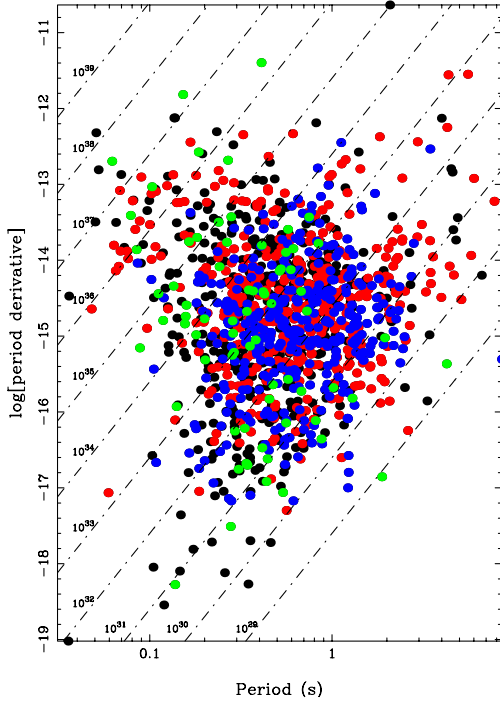


Figure 4. The period-period derivative plane of the pulsars in the sample (black). The RVM class are shown in red, the ‘flat’ class in green and the non-RVM in blue. Lines of constant \dot{E} are shown with dash-dots.

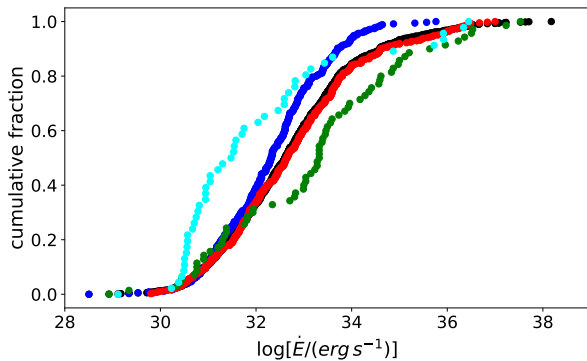


Figure 5. Cumulative \dot{E} distributions for the whole sample (black), the RVM class (red), the non-RVM class (blue), the flat class (green) and pulsars with low values of α (cyan).

flat PA swings, low \dot{E} and relatively high linear polarization fraction. Some of these pulsars have profiles with very large widths such as PSRs J1232–4742 (Figure 2) and J1842+1332; presumably these are nearly aligned rotators where the line of sight remains within the beam. This is reminiscent of the profiles of radio-loud magnetars such as XTE J1810–197 (Camilo et al. 2007) and PSR J1622–4950 (Levin et al. 2012). Others such as PSRs J0108–1431 and J1511–5414 (both shown in Figure 2) have narrow profiles, either because the line-of-sight just grazes the beam edge or because the emission is from an isolated patch far from the magnetic axis on the leading or trailing edges.

5.3 Relativistic effects

More than 30 years ago, Blaskiewicz et al. (1991) pointed out that the inflection point of the RVM curve (ϕ_0) should trail the centroid of the intensity profile by an amount which depends linearly on the rotation period and the emission height. For the pulsars in our sample we define the centroid as lying half-way between the 10% intensity levels of the profile, which we label ϕ_m . Then, $\Delta\phi$ is simply $\phi_0 - \phi_m$ which can be related to the physical parameters via Equation 4.

We find that $\Delta\phi$ is within 1° of zero in 20% of cases, $\Delta\phi > 1^\circ$ in 62% of pulsars and $\Delta\phi < -1^\circ$ for 18% of the population (see Table 1). This strong bias towards positive values indicates the Blaskiewicz et al. (1991) effect at work. Figure 6 shows $\Delta\phi/W$ versus \dot{E} . Here we see that virtually all pulsars with $\dot{E} > 10^{34}$ erg s $^{-1}$ have $\Delta\phi/W > 0^\circ$ (53 out of 61 cases). This is likely due to a combination of short P and high heights (cf Equation 4). For pulsars with $\dot{E} < 10^{34}$ erg s $^{-1}$ there remains a strong bias towards positive values of $\Delta\phi/W$ (262 out of 350 cases). Some of the pulsars with negative $\Delta\phi$ are so-called ‘partial cones’ which are dealt with in more detail in subsection 5.6.

5.4 Emission Heights

We can compute a limit on the emission height for the pulsars in the RVM class in the following (geometric) way. If we assume that the beams are filled and that $\alpha = 90^\circ$ for all pulsars, an upper limit on the emission height is given by Equations 2 and 3. The resultant histogram of heights computed in this way is shown in Figure 7. From this figure we see that 35% of the pulsars have $h_{\max} < 300$ km and 77% have $h_{\max} < 1000$ km. This provides strong evidence that the radio emission from pulsars arises from low altitude, and does not depend greatly on the spin period (Johnston & Karastergiou 2019; Posselt et al. 2021). In addition we also note that pulsars with apparent $h_{\max} > 1000$ km have predominantly low values of \dot{E} . Given that α evolves with time, these pulsars likely have α significantly less than 90° and as a result lower emission heights than h_{\max} .

We can also compute emission heights using the relativistic effects described in the previous subsection. Knowledge of $\Delta\phi_0$ can be converted to a height using Equation 4. We find that, at most, only 10% of the pulsars can have $h_{\max} > 1000$ km when measured in this way. In summary therefore, the geometric approach and the relativistic approach give reasonable agreement and we surmise that virtually all the pulsars in this sample have $h_{\max} < 1000$ km, independent of spin period.

5.4.1 Pulsars with high \dot{E}

There are 55 pulsars in the sample with $\dot{E} > 10^{35}$ erg s $^{-1}$, only 5 of which are in the non-RVM class. A high fraction of these pulsars are seen at X-ray and/or γ -ray energies. In the outer-gap or two-pole caustic model of γ -ray emission (Dyks & Rudak 2003; Watters & Romani 2011) the expectation is that these pulsars are predominantly seen at high values of α . In addition if α is randomly distributed at birth, then geometrical considerations again imply that high values of α should dominate in the observed population. However, a comprehensive study of these pulsars by Rookyard et al. (2015a,b) showed that either the α distribution is skewed towards low values or emission must arise from an open field-line region which is larger than conventionally defined from equation 2.

Recent work on γ -ray emission models (Pétri & Mitra 2021) have shown that high values of α may not be necessary (Dirson et al. 2022). A study of interpulse pulsars with high \dot{E} (Johnston & Kramer 2019) showed that low emission heights are prevalent and that in many

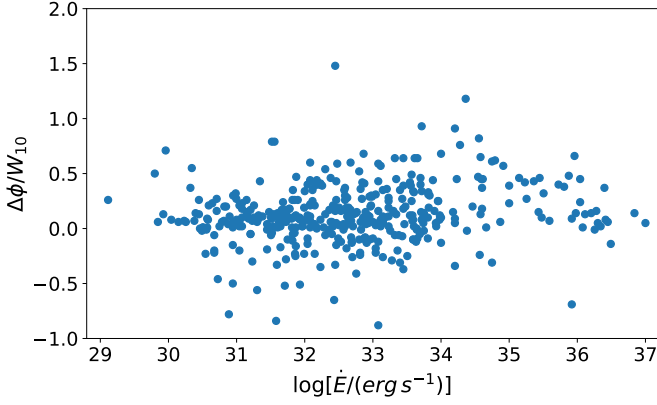


Figure 6. Spin-down energy loss-rate \dot{E} versus $\Delta\phi/W_{10}$ for a sample of 411 pulsars. See text for details.

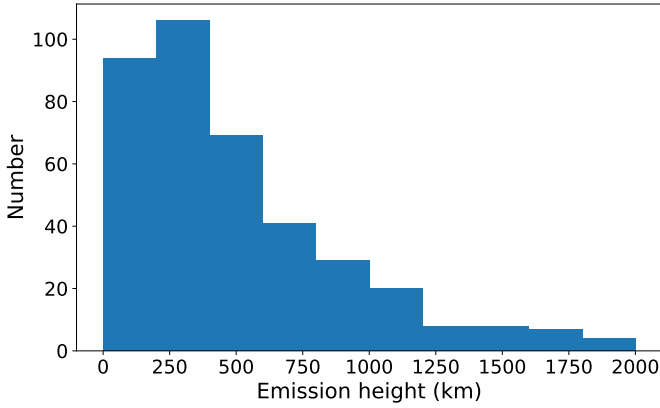


Figure 7. Histogram of the emission heights of 386 pulsars with good RVM fits under the assumptions that $\alpha = 90^\circ$ and that the beams are filled. A further 35 pulsars with $h_{\max} > 2000$ km are not shown.

instances the beam is underfilled. In the work presented here, the measured values of $\Delta\phi$ also generally prefer low emission heights (below 500 km). These low emission heights coupled with large widths again imply low values of α via equation 3. We are therefore forced into the same conclusion as Rookyard et al. (2015a) that either α is not randomly distributed or that emission occurs over a larger region than the classic polar cap extent. Indeed in a force-free magnetosphere the closed field-line region does not reach the light cylinder, thereby extending the region bounded by the open field lines (e.g. Spitkovsky 2006; Craig 2014; Philippov & Kramer 2022). Additional theoretical support for this idea based on the phenomenology of sub-pulse drifting can be found in Wright (2022).

5.5 Evidence for evolution of α with time

In the previous section we showed strong evidence that emission heights are less than 1000 km for the majority of the radio pulsar population. If we now **assume** that 1000 km is the maximum allowed emission height, then we can use the width of the profile to provide an upper limit on the value of α by combining equations 2 and 3. As an example, it can be seen that for PSR J1842–0359 in Figure 1 the maximum value of α is 15° . Of the 431 pulsars with good RVM fits,

47 have a maximum allowed α less than 45° . The cumulative \dot{E} distribution of these pulsars is shown in cyan on Figure 5. The distribution is dominated by low \dot{E} pulsars, 37 of the 47 have $\dot{E} < 10^{33}$ erg s $^{-1}$ and only 5 have $\dot{E} > 10^{35.5}$ erg s $^{-1}$. As lower \dot{E} pulsars are older than those with higher \dot{E} , this result supports an evolution of the magnetic axis towards the spin axis with time, evidence for which is also apparent in other observational studies (Tauris & Manchester 1998; Weltevrede & Johnston 2008a; Johnston & Karastergiou 2017) with theoretical underpinning in Philippov et al. (2014) and Novoselov et al. (2020).

5.6 Partial Cones?

If the pulsar beam consists of nested cones, as in Rankin (1990), there may be instances where the leading or trailing part of the cone is below the detection threshold and this would manifest itself as a ‘partial cone’ in the nomenclature of Lyne & Manchester (1988). In the patchy beam model similarly there may be occasions in which only the leading or trailing part of the beam is illuminated. In the study of 200 pulsars by Lyne & Manchester (1988) they found up to 50 pulsars (25%) could be classified as partial cones with a ratio of approximately 2:1 between pulsars where only the leading edge is seen compared to the trailing edge. These results were obtained largely by comparing the inflection point of the PA swing to the midpoint of the pulse profile. A few years later, Blaskiewicz et al. (1991) pointed out that, due to finite emission heights, it was expected that the PA swing would be delayed compared to the pulse profile midpoint. In retrospect therefore, we see that many (perhaps all) of the leading partial cones in Lyne & Manchester (1988) are mis-classified once these relativistic effects are taken into account. Furthermore, more sensitive observations carried out on the Lyne & Manchester (1988) sample by Mitra & Rankin (2011) concluded that there were no good examples of the inflection point leading the profile midpoint and that trailing partial cones were not seen.

We largely concur that none of the pulsars identified in Lyne & Manchester (1988) are convincing as trailing partial cones. However, we find several striking examples of this amongst our sample from pulsars discovered post-1988. The most prominent examples are PSRs J0134–2937, J1648–6044 (both shown in Figure 8) and J2234+2114 with perhaps 2-3 other less convincing cases. In total therefore the trailing partial cones form only a very small minority (< 5%) of the overall population. For pulsars which have ϕ_0 later than the profile midpoint, the majority can be put down to aberration and retardation effects. An example is PSR J0631+1036 (Figure 8) which has a beautifully symmetric four-component profile yet ϕ_0 occurs significantly later than the symmetric midpoint. Perhaps the two best examples of potential leading partial cones are PSRs J1615–5444 (Figure 8) and J1847–0605 but again the fraction of this type of pulsar in the data is very low.

This should not be taken to mean that all pulsar profiles show symmetrical emission patterns about both sides of the magnetic pole. That this is not the case is seen most obviously in the Vela pulsar which clearly lacks emission in the trailing part of the cone. Some of the pulsars with interpulse emission also have highly non-symmetrical emission patterns (see Johnston & Kramer 2019).

5.7 Orthogonal mode jumps

The presence of two orthogonally polarized emission modes in pulsar profiles has been known since the 1970s (Backer et al. 1976). If the dominant emission mode changes across the profile, a 90° jump in

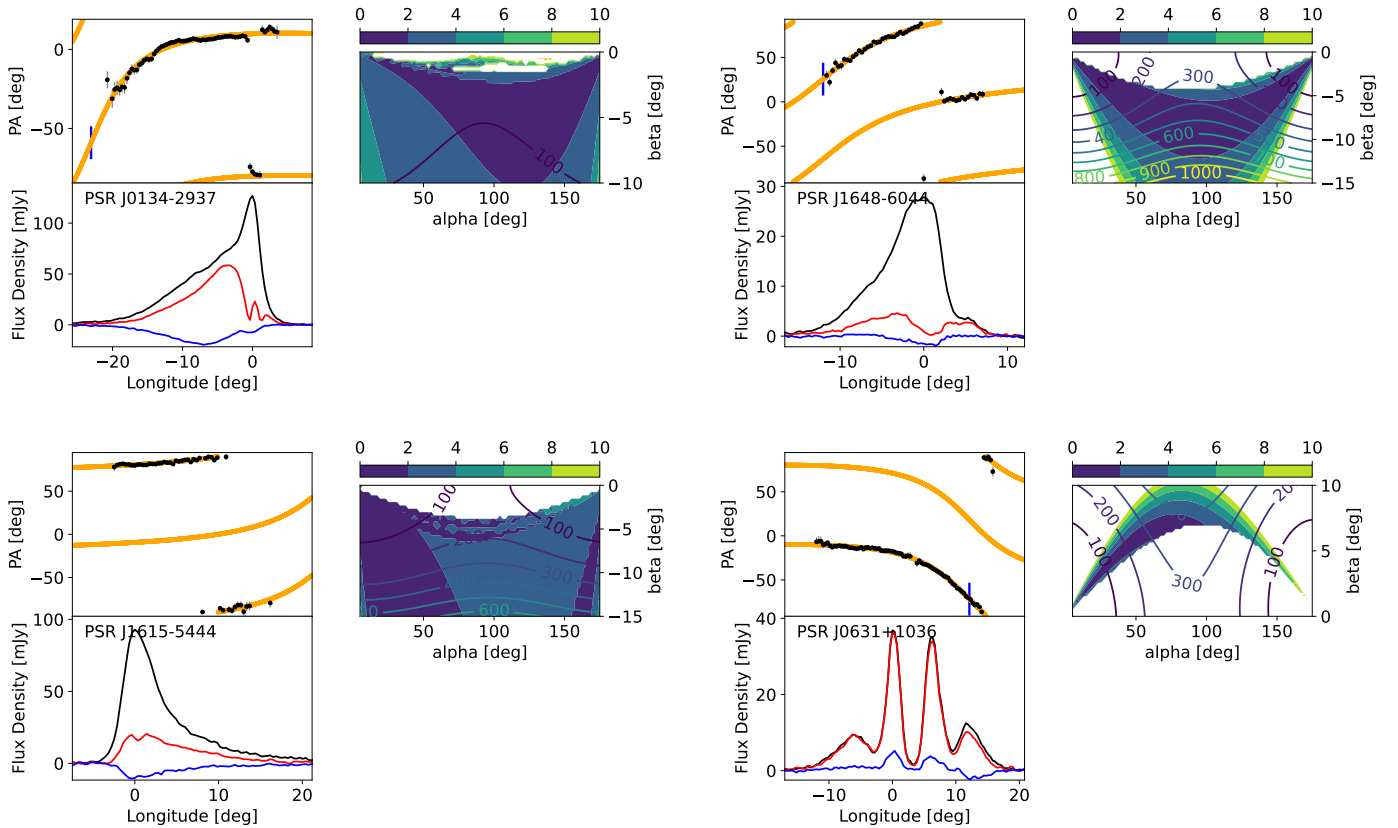


Figure 8. Two examples of trailing partial cone pulsars are PSRs J0134–2937 (top left) and J1648–6044 (top right). In these two cases ϕ_0 occurs significantly earlier than the profile midpoint and the profile has a lop-sided look. An example of a leading partial cone is PSR J1615–5444 (bottom left). Finally PSR J0631+1035 (bottom right) is an example of a symmetrical profile with ϕ_0 shifted later due to relativistic effects.

the PA swing is observed (e.g. PSR J1110–5637 in Figure 1). If we examine the profiles of all the pulsars in the ‘RVM’ and ‘flat’ class, we find that at least one orthogonal jump occurs in 139 out of 502 cases (28%). We see that the prevalence of orthogonal jumps is lower in the pulsars with a high \dot{E} , with only 8 out of 81 pulsars with $\dot{E} > 10^{34}$ erg s $^{-1}$ showing this effect. We note that the fraction of pulsars showing an orthogonal jump should be considered a lower limit. Some of the pulsars in the ‘non-RVM’ category show ‘resolved’ jumps (e.g. PSR J0738–4042; see Figure 9) and some show jumps which differ from 90° by enough to render the RVM fit poor.

We note that, from these data alone, we cannot tell which is the prevalent dominant mode in the population as a whole. When combined with proper motion information, Johnston et al. (2005), Rankin (2007) and Noutsos et al. (2012) have shown that in some cases the emission parallel to the magnetic field lines dominate while in yet others the perpendicular emission is the dominant one.

6 CONCLUSIONS

The Thousand Pulsar Array programme on the MeerKAT telescope has produced a homogenous set of data on more than 1200 pulsars as detailed in Posselt et al. (2022). We have used the calibrated polarization profiles to perform RVM fits to 854 pulsars. Our main findings are:

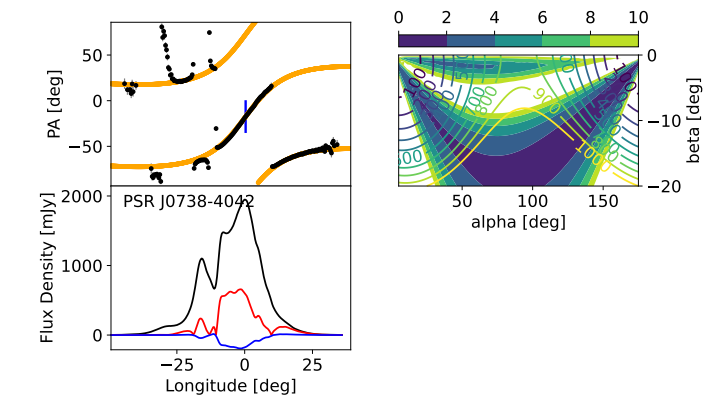


Figure 9. PSR J0738–4042, an example of a pulsar with orthogonal mode jumps which are not instantaneous but resolved in phase. This causes the RVM fitter to return a high value of χ^2 .

- (i) Some 60% of pulsars have PA traverses which are amenable to RVM fits.
- (ii) For the 40% of pulsars for which the RVM fit fails, a substantial number have a circular polarization fraction which exceeds that of the linear polarization in more than 5 bins across the profile. We

surmise that coherent mixing of the linearly polarized modes may be responsible.

(iii) From geometrical considerations alone, the emission height of the radio radiation at 1.4 GHz is less than 1000 km and is largely independent of rotation period. Emission heights obtained through relativistic delay of the polarization with respect to the total intensity emission also show that emission heights must be low.

(iv) There remains a problem with the high \dot{E} pulsars; either their α distribution is non-random or emission occurs from outside the conventionally defined polar cap.

(v) Under the assumption that emission heights are less than 1000 km across the population then there is strong evidence for alignment of the magnetic and rotation axes.

(vi) The dominant emission mode changes across the profile in at least 28% of the population, a fraction which is lower in the high \dot{E} pulsars.

(vii) Clear examples of partial cones are rare in the population as a whole.

DATA AVAILABILITY

The complete set of pulsar profiles used in this work is available under the DOI 10.5281/zenodo.7272361, with all details to be found in [Posselt et al. \(2022\)](#).

ACKNOWLEDGEMENTS

The MeerKAT telescope is operated by the South African Radio Astronomy Observatory, which is a facility of the National Research Foundation, an agency of the Department of Science and Innovation. MeerTime data is housed and processed on the OzSTAR supercomputer at Swinburne University of Technology with the support of ADACS and the gravitational wave data centre via AAL. LSO acknowledges the support of Magdalen College, Oxford.

REFERENCES

- Backer D. C., Rankin J. M., Campbell D. B., 1976, *Nature*, 263, 202
 Bailes M., et al., 2020, *PASA*, 37, e028
 Beskin V. S., Philippov A. A., 2012, *MNRAS*, 425, 814
 Blaskiewicz M., Cordes J. M., Wasserman I., 1991, *ApJ*, 370, 643
 Camilo F., Reynolds J., Johnston S., Halpern J. P., Ransom S. M., van Straten W., 2007, *ApJ*, 659, L37
 Craig H. A., 2014, *ApJ*, 790, 102
 Craig H. A., Romani R. W., 2012, *ApJ*, 755, 137
 Desvignes G., Kramer M., Lee K., et al. 2019, *Science*, 365, 1013
 Dirson L., Pétri J., Mitra D., 2022, *A&A*, 667, A82
 Dyks J., 2017, *MNRAS*, 471, L131
 Dyks J., 2019, *MNRAS*, 488, 2018
 Dyks J., 2020, *MNRAS*, 495, L118
 Dyks J., Rudak B., 2003, *ApJ*, 598, 1201
 Dyks J., Rudak B., 2015, *MNRAS*, 446, 2505
 Everett J. E., Weisberg J. M., 2001, *ApJ*, 553, 341
 Fussell D., Luo Q., 2004, *MNRAS*, 349, 1019
 Gangadhara R. T., 2004, *ApJ*, 609, 335
 Gil J., Gronkowski P., Rudnicki W., 1984, *A&A*, 132, 312
 Hotan A. W., van Straten W., Manchester R. N., 2004, *PASA*, 21, 302
 Ilie C. D., Johnston S., Weltevrede P., 2019, *MNRAS*, 483, 2778
 Johnston S., Karastergiou A., 2017, *MNRAS*, 467, 3493
 Johnston S., Karastergiou A., 2019, *MNRAS*, 485, 640
 Johnston S., Kramer M., 2019, *MNRAS*, 490, 4565
 Johnston S., Weisberg J. M., 2006, *MNRAS*, 368, 1856

- Johnston S., Hobbs G., Vigeland S., Kramer M., Weisberg J. M., Lyne A. G., 2005, *MNRAS*, 364, 1397
 Johnston S., et al., 2020, *MNRAS*, 493, 3608
 Karastergiou A., 2009, *MNRAS*, 392, L60
 Karastergiou A., Johnston S., 2007, *MNRAS*, 380, 1678
 Kennett M., Melrose D., 1998, *PASA*, 15, 211
 Levin L., et al., 2012, *MNRAS*, 422, 2489
 Lockhart W., Gralla S. E., Özel F., Psaltis D., 2019, *MNRAS*, 490, 1774
 Lyne A. G., Manchester R. N., 1988, *MNRAS*, 234, 477
 Mitra D., Rankin J. M., 2002, *ApJ*, 577, 322
 Mitra D., Rankin J. M., 2011, *ApJ*, 727, 92
 Noutsos A., Kramer M., Carr P., Johnston S., 2012, *MNRAS*, 423, 2736
 Novoselov E. M., Beskin V. S., Galishnikova A. K., Rashkovetskiy M. M., Biryukov A. V., 2020, *MNRAS*, 494, 3899
 Oswald L., Karastergiou A., Johnston S., 2019, *MNRAS*, 489, 310
 Oswald L. S., et al., 2021, *MNRAS*, 504, 1115
 Oswald L., Johnston S., Karastergiou A., Dai S., Kerr M., Lower M. E., Shannon R. M., Weltevrede P., 2022, *MNRAS*, In Press
 Parthasarathy A., et al., 2021, *MNRAS*, 502, 407
 Pétri J., 2020, *MNRAS*, 499, 4445
 Pétri J., Mitra D., 2021, *A&A*, 654, A106
 Philippov A., Kramer M., 2022, *ARA&A*, 60, 495
 Philippov A., Tchekhovskoy A., Li J. G., 2014, *MNRAS*, 441, 1879
 Posselt B., et al., 2021, *MNRAS*, 508, 4249
 Posselt B., et al., 2022, *MNRAS*, In Press
 Radhakrishnan V., Cooke D. J., 1969, *Astrophysics Letters*, 3, 225
 Radhakrishnan V., Rankin J. M., 1990, *ApJ*, 352, 258
 Rankin J. M., 1983, *ApJ*, 274, 333
 Rankin J. M., 1990, *ApJ*, 352, 247
 Rankin J. M., 2007, *ApJ*, 664, 443
 Rookyard S. C., Weltevrede P., Johnston S., 2015a, *MNRAS*, 446, 3356
 Rookyard S. C., Weltevrede P., Johnston S., 2015b, *MNRAS*, 446, 3367
 Serylak M., et al., 2021, *MNRAS*, 505, 4483
 Spitkovsky A., 2006, *ApJ*, 648, L51
 Tauris T. M., Manchester R. N., 1998, *MNRAS*, 298, 625
 Wang H. G., et al., 2014, *ApJ*, 789, 73
 Watters K. P., Romani R. W., 2011, *ApJ*, 727, 123
 Weltevrede P., Johnston S., 2008a, *MNRAS*, 387, 1755
 Weltevrede P., Johnston S., 2008b, *MNRAS*, 391, 1210
 Weltevrede P., Wright G., 2009, *MNRAS*, 395, 2117
 Weltevrede P., Stappers B. W., van den Horn L. J., Edwards R. T., 2003, *A&A*, 412, 473
 Wright G., 2022, *MNRAS*, 514, 4046
 Yuen R., Melrose D. B., 2014, *PASA*, 31, e039

APPENDIX A: TABLES

This paper has been typeset from a $\text{\TeX}/\text{\LaTeX}$ file prepared by the author.

Table A1. Pulsars classified as RVM. The sign of β is given in column 3. Column 4 indicates whether $V > L$ in more than 5 phase bins across the profile. Column 5 indicates the offset between ϕ_0 and the profile midpoint. Interpulse pulsars are denoted with an M (main pulse) or I (interpulse) suffix.

JNAME	BNAME	β	V_h	$\Delta\phi$										
J0045–7042		+ve	no	+ve	J0134–2937		–ve	no	–ve	J0151–0635	B0148–06	–ve	no	0
J0304+1932	B0301+19	+ve	no	0	J0343–3000		–ve	no	+ve	J0452–1759	B0450–18	–ve	yes	+ve
J0459–0210		+ve	yes	–ve	J0514–4407M		+ve	no	+ve	J0534–6703		–ve	no	+ve
J0536–7543	B0538–75	+ve	no	0	J0543+2329	B0540+23	+ve	no	+ve	J0555–7056		–ve	no	+ve
J0614+2229	B0611+22	–ve	no	+ve	J0627+0649		+ve	no	+ve	J0627+0706I		–ve	no	0
J0627+0706M		–ve	no	–ve	J0630–2834	B0628–28	+ve	no	0	J0631+1036		+ve	no	+ve
J0633–2015		–ve	no	0	J0646+0905		+ve	no	–ve	J0659+1414	B0656+14	+ve	no	+ve
J0709–5923		+ve	no	–ve	J0711+0931		–ve	no	0	J0729–1448		–ve	no	+ve
J0729–1836	B0727–18	–ve	no	+ve	J0737–2202		–ve	no	+ve	J0742–2822	B0740–28	+ve	no	+ve
J0812–3905		–ve	no	+ve	J0818–3049		–ve	no	+ve	J0820–3921		+ve	no	+ve
J0821–4221		+ve	no	+ve	J0831–4406		+ve	no	0	J0835–4510	B0833–45	+ve	no	+ve
J0837–2454		–ve	yes	+ve	J0838–2621		–ve	no	+ve	J0842–4851M	B0840–48M	–ve	no	–ve
J0843–5022		–ve	yes	+ve	J0847–4316		–ve	no	0	J0849–6322		+ve	no	–ve
J0855–4644		–ve	no	+ve	J0855–4658		+ve	no	–ve	J0856–6137	B0855–61	–ve	no	–ve
J0857–4424		+ve	no	–ve	J0901–4624		+ve	yes	+ve	J0904–4246	B0903–42	+ve	no	0
J0904–7459	B0904–74	–ve	no	–ve	J0905–4536		+ve	no	+ve	J0905–5127M		–ve	no	+ve
J0905–6019		+ve	yes	0	J0907–5157	B0905–51	–ve	no	–ve	J0908–4913I	B0906–49I	–ve	no	+ve
J0908–4913M	B0906–49M	+ve	no	+ve	J0909–7212	B0909–71	+ve	no	+ve	J0912–3851		+ve	yes	0
J0922+0638	B0919+06	–ve	no	+ve	J0924–5814	B0923–58	+ve	no	+ve	J0932–3217		–ve	no	0
J0932–5327		–ve	no	0	J0940–5428		–ve	no	+ve	J0942–5657	B0941–56	–ve	no	0
J0943+1631	B0940+16	–ve	no	+ve	J0945–4833		+ve	no	+ve	J0952–3839	B0950–38	–ve	no	–ve
J0954–5430		–ve	no	0	J0957–5432		–ve	no	+ve	J0959–4809	B0957–47	–ve	yes	0
J1000–5149		+ve	no	–ve	J1001–5939		+ve	no	0	J1002–5919		+ve	no	+ve
J1012–2337	B1010–23	+ve	no	+ve	J1013–5934		–ve	no	+ve	J1015–5719		–ve	no	+ve
J1016–5345	B1014–53	–ve	no	+ve	J1016–5857		+ve	no	+ve	J1020–5921		–ve	no	0
J1032–5206		–ve	no	0	J1038–5831	B1036–58	–ve	no	0	J1041–1942	B1039–19	+ve	no	+ve
J1042–5521	B1039–55	–ve	no	+ve	J1048–5832	B1046–58	–ve	no	0	J1049–5833		–ve	no	–ve
J1052–6348		+ve	no	–ve	J1054–6452		+ve	no	–ve	J1055–6028		+ve	no	0
J1055–6905		+ve	no	–ve	J1057–5226M	B1055–52M	–ve	no	–ve	J1057–7914	B1056–78	–ve	no	0
J1103–6025		–ve	no	+ve	J1104–6103		–ve	no	+ve	J1105–6107		–ve	no	+ve
J1110–5637	B1107–56	–ve	no	+ve	J1114–6100	B1112–60	+ve	no	–ve	J1115–6052		+ve	no	+ve
J1116–4122	B1114–41	+ve	no	–ve	J1117–6154		+ve	no	0	J1119–7936	B1118–79	–ve	no	0
J1123–6102		–ve	yes	+ve	J1123–6259		+ve	no	–ve	J1124–5638		–ve	yes	–ve
J1126–6942		+ve	no	–ve	J1132–4700		–ve	no	+ve	J1141–3107		+ve	no	–ve
J1141–6545		–ve	yes	+ve	J1143–5536		–ve	no	0	J1146–6030	B1143–60	+ve	no	+ve
J1148–5725		+ve	no	0	J1151–6108		–ve	no	+ve	J1152–6012		+ve	no	–ve
J1159–6409		–ve	no	0	J1204–6843		+ve	yes	+ve	J1211–6324		–ve	no	+ve
J1215–5328		+ve	yes	+ve	J1220–6318		+ve	no	+ve	J1222–5738		–ve	yes	–ve
J1224–6208		–ve	no	+ve	J1236–5033		–ve	no	+ve	J1245–6238		+ve	yes	0
J1252–6314		+ve	no	–ve	J1253–5820		–ve	no	+ve	J1254–6150		+ve	no	–ve
J1301–6310		–ve	no	+ve	J1302–6350	B1259–63	–ve	no	–ve	J1305–6203		+ve	no	–ve
J1308–4650		–ve	no	0	J1311–1228	B1309–12	+ve	no	–ve	J1312–5402	B1309–53	–ve	no	0
J1312–5516	B1309–55	–ve	no	0	J1319–6105		–ve	no	–ve	J1320–5359	B1317–53	+ve	no	+ve
J1326–6700	B1322–66	–ve	no	0	J1327–6301	B1323–627	+ve	no	+ve	J1328–4357	B1325–43	–ve	no	0
J1331–5245		+ve	yes	0	J1339–6618		–ve	no	+ve	J1340–6456	B1336–64	–ve	yes	+ve
J1345–6115		+ve	yes	0	J1350–5115		+ve	no	–ve	J1352–6803		+ve	no	–ve
J1357–6429		–ve	no	–ve	J1401–6357	B1358–63	–ve	no	0	J1403–6310		–ve	no	+ve
J1403–7646		+ve	no	+ve	J1404+1159		+ve	no	0	J1412–6111		+ve	no	0
J1413–6307I	B1409–62I	+ve	no	–ve	J1414–6802		–ve	no	0	J1415–6621		+ve	no	+ve
J1416–6037		–ve	no	+ve	J1420–6048		–ve	no	+ve	J1424–5556		–ve	no	–ve
J1424–6438		+ve	no	0	J1425–6210		–ve	no	–ve	J1427–4158		–ve	no	0
J1428–5530	B1424–55	–ve	yes	0	J1432–5032		–ve	no	–ve	J1435–5954		–ve	no	+ve
J1443–5122		–ve	no	0	J1452–5851		+ve	no	+ve	J1502–5653		+ve	no	+ve
J1502–6128		+ve	no	+ve	J1507–4352	B1504–43	+ve	no	+ve	J1512–5431		+ve	no	0
J1513–5739		–ve	no	0	J1517–4636		–ve	no	+ve	J1518–0627		–ve	no	–ve

Table A1. Pulsars classified as RVM (continued).

JNAME	BNAME	β	V_h	$\Delta\phi$										
J1519–6106		–ve	no	+ve	J1519–6308		–ve	no	+ve	J1522–5525		+ve	no	0
J1524–5819		–ve	no	–ve	J1527–3931	B1524–39	+ve	yes	0	J1530–5327		–ve	no	0
J1531–4012		+ve	no	0	J1535–4114		–ve	no	+ve	J1535–4415		–ve	no	–ve
J1535–5848		+ve	no	+ve	J1537–4912		+ve	no	+ve	J1537–5153		–ve	no	0
J1538+2345		–ve	no	0	J1538–5732		–ve	no	+ve	J1539–4828		+ve	no	0
J1539–6322		+ve	no	0	J1542–5303		+ve	no	+ve	J1543–5013		–ve	no	0
J1548–4927		–ve	no	+ve	J1549+2113		–ve	no	–ve	J1549–4848I		–ve	no	+ve
J1550–5242		–ve	no	+ve	J1554–5209		+ve	no	0	J1555–2341	B1552–23	–ve	no	+ve
J1558–5756		+ve	no	0	J1559–4438	B1556–44	+ve	yes	–ve	J1601–5335		–ve	no	+ve
J1603–5657		–ve	no	–ve	J1605–5257	B1601–52	+ve	no	+ve	J1611–4949		–ve	no	–ve
J1614+0737	B1612+07	+ve	no	–ve	J1614–3937		+ve	yes	0	J1615–5444		–ve	no	+ve
J1616–5017		–ve	yes	0	J1617–4216		–ve	no	0	J1622–3751		+ve	no	0
J1622–4347		–ve	no	+ve	J1622–4802		+ve	no	–ve	J1622–4950		–ve	yes	–ve
J1623–4949		–ve	no	–ve	J1626–4537		–ve	no	–ve	J1632–1013		+ve	no	+ve
J1634–5640		+ve	no	0	J1635–4944		+ve	no	–ve	J1636–2614		–ve	no	+ve
J1637–4642		+ve	no	+ve	J1638–3951		+ve	no	–ve	J1638–4344		+ve	no	0
J1646–5123		–ve	no	+ve	J1648–6044		–ve	yes	–ve	J1653–3838	B1650–38	–ve	no	–ve
J1655–3844		–ve	yes	0	J1656–3621		–ve	no	+ve	J1700–3312		–ve	no	0
J1700–3919		+ve	yes	0	J1703–1846	B1700–18	+ve	no	+ve	J1703–3241	B1700–32	–ve	no	0
J1703–4442		–ve	no	0	J1704–5236		+ve	no	–ve	J1705–3950		+ve	yes	+ve
J1707–4341		+ve	yes	+ve	J1707–4417		–ve	no	0	J1709–1640	B1706–16	+ve	no	0
J1709–3626		–ve	no	0	J1709–4401		–ve	no	0	J1711–1509	B1709–15	–ve	yes	+ve
J1716–4711		+ve	yes	0	J1718–3825		–ve	no	+ve	J1719–4302		+ve	no	+ve
J1720–0212	B1718–02	+ve	yes	+ve	J1720–1633	B1717–16	–ve	no	0	J1720–2933	B1717–29	+ve	yes	0
J1722–3207	B1718–32	+ve	no	–ve	J1722–3712I	B1719–37I	–ve	no	+ve	J1722–3712M	B1719–37M	–ve	no	+ve
J1722–4400		+ve	no	0	J1723–3659		+ve	yes	+ve	J1727–2739		–ve	no	+ve
J1728–0007	B1726–00	–ve	no	–ve	J1733–3716	B1730–37	+ve	yes	+ve	J1733–4005		–ve	yes	–ve
J1734–0212	B1732–02	–ve	yes	0	J1737–3102		+ve	yes	–ve	J1737–3555	B1734–35	+ve	no	0
J1738–2955		+ve	no	–ve	J1739–2903I	B1736–29I	+ve	no	+ve	J1739–3023		–ve	no	+ve
J1740+1000		–ve	no	+ve	J1740+1311	B1737+13	+ve	no	+ve	J1740–3015	B1737–30	+ve	yes	+ve
J1741–0840	B1738–08	–ve	no	0	J1743–0339	B1740–03	–ve	no	+ve	J1743–3150	B1740–31	–ve	no	0
J1743–4212		–ve	no	+ve	J1744–3130		+ve	no	+ve	J1745–3812		–ve	no	0
J1746+2245		–ve	yes	–ve	J1748–1300	B1745–12	+ve	yes	+ve	J1750–3503		+ve	no	–ve
J1751–3323		+ve	no	–ve	J1754–3443		+ve	yes	–ve	J1757–1500		–ve	yes	+ve
J1759–3107		+ve	no	+ve	J1800–0125		+ve	no	+ve	J1801–2920	B1758–29	–ve	yes	0
J1802+0128		+ve	no	–ve	J1803–2137	B1800–21	+ve	no	+ve	J1806–1154	B1804–12	+ve	yes	0
J1808–0813		+ve	no	–ve	J1808–3249		+ve	no	+ve	J1809–1429		–ve	yes	–ve
J1809–1917		+ve	no	–ve	J1809–1943		+ve	yes	+ve	J1809–2109	B1806–21	–ve	no	0
J1810–5338	B1806–53	–ve	no	0	J1813–2113		–ve	no	–ve	J1816–0755M		–ve	no	0
J1817–3618	B1813–36	–ve	yes	+ve	J1819+1305		–ve	no	+ve	J1819–0925		+ve	no	0
J1819–1008		+ve	no	–ve	J1819–1458		–ve	no	0	J1821–0331		–ve	no	–ve
J1823–0154		+ve	no	+ve	J1823–3106	B1820–31	+ve	no	+ve	J1824–0127		–ve	no	+ve
J1826–1334	B1823–13	+ve	yes	+ve	J1828+1359		+ve	yes	–ve	J1830–1059	B1828–11	+ve	no	+ve
J1831–0823		–ve	yes	0	J1831–0952		–ve	no	+ve	J1835–0349		–ve	yes	+ve
J1835–0944		+ve	no	–ve	J1835–1020		+ve	no	0	J1835–1106		–ve	no	+ve
J1837+1221		+ve	no	0	J1837–0045		+ve	no	–ve	J1837–1837		+ve	no	+ve
J1839–0436		+ve	yes	+ve	J1839–1238		+ve	yes	–ve	J1840+0214		–ve	no	–ve
J1840–0809		–ve	no	+ve	J1840–1122		–ve	no	+ve	J1841+0912	B1839+09	+ve	no	0
J1841–0345		–ve	no	+ve	J1841–0524		+ve	no	+ve	J1842+0257		+ve	no	0
J1842+0358		–ve	no	–ve	J1842+0638		+ve	no	–ve	J1842–0359	B1839–04	–ve	no	0
J1842–0905		–ve	yes	+ve	J1843–0000		+ve	no	+ve	J1843–0211		–ve	no	0
J1843–0702I		+ve	no	–ve	J1843–0806		+ve	no	–ve	J1845–0434	B1842–04	–ve	yes	0
J1845–0545		+ve	no	–ve	J1845–0635		+ve	no	–ve	J1845–1114		–ve	no	+ve
J1846+0051		+ve	no	+ve	J1846–07492		+ve	yes	0	J1847–0438		–ve	no	–ve
J1847–0605		+ve	no	+ve	J1848+0604		–ve	yes	+ve	J1849+0409M		–ve	no	+ve

Table A1. Pulsars classified as RVM (continued).

JNAME	BNAME	β	V_h	$\Delta\phi$										
J1849+2423		+ve	no	+ve	J1849-0317		-ve	no	0	J1849-0614		+ve	no	+ve
J1850+0026		+ve	yes	-ve	J1850+1335	B1848+13	+ve	no	0	J1851+1259	B1848+12	-ve	no	0
J1851-0053		+ve	yes	0	J1852-0635		+ve	no	0	J1854+0319		+ve	yes	-ve
J1854-1421	B1851-14	+ve	no	-ve	J1855+0307		-ve	no	0	J1855-0941		-ve	no	+ve
J1856-0526		-ve	yes	+ve	J1857+0057	B1854+00	-ve	no	+ve	J1900-0051		-ve	no	+ve
J1900-0933		+ve	no	-ve	J1901+0124		-ve	no	+ve	J1901+0234		+ve	no	+ve
J1901+0716	B1859+07	-ve	no	-ve	J1901+1306		-ve	no	0	J1901-0312		+ve	no	+ve
J1902+0615	B1900+06	-ve	no	-ve	J1903+2225		-ve	no	0	J1903-0632	B1900-06	+ve	no	+ve
J1903-0848		+ve	no	+ve	J1904+1011	B1901+10	+ve	no	+ve	J1905+0616		+ve	no	0
J1905+0709	B1903+07	-ve	no	+ve	J1907+0631		+ve	no	+ve	J1907+0740		-ve	no	+ve
J1907+0918		-ve	yes	0	J1907+1149		-ve	no	+ve	J1908+0500		+ve	no	+ve
J1909+0749I		+ve	no	-ve	J1909+0749M		-ve	no	+ve	J1910+0728		-ve	yes	0
J1911+1758		+ve	no	-ve	J1912+2104	B1910+20	-ve	no	0	J1913+0936	B1911+09	-ve	no	+ve
J1914+0219		+ve	no	0	J1914+1122	B1911+11	+ve	no	0	J1915+0738		-ve	no	+ve
J1915+0752		+ve	no	+ve	J1915+1606	B1913+16	-ve	no	+ve	J1915+1647	B1913+167	+ve	no	0
J1916+1312	B1914+13	-ve	yes	+ve	J1917+0834		-ve	no	0	J1917+1353	B1915+13	+ve	no	+ve
J1918+1444	B1916+14	-ve	no	0	J1918+1541M		-ve	no	-ve	J1918-1052		-ve	yes	+ve
J1919+1745		-ve	no	0	J1920-0950		-ve	no	+ve	J1921+0812		-ve	no	+ve
J1921+1419	B1919+14	+ve	no	+ve	J1922+1733		+ve	no	+ve	J1924+1631		-ve	no	-ve
J1925+1720		+ve	no	+ve	J1926+1434	B1924+14	-ve	yes	+ve	J1926+1648	B1924+16	-ve	no	+ve
J1926+2016		+ve	no	+ve	J1926-0652		+ve	no	0	J1927+1852	B1925+18	+ve	no	+ve
J1927+2234	B1925+22	-ve	no	0	J1928+1746		-ve	no	+ve	J1931+1439		+ve	no	0
J1931+1536	B1929+15	-ve	no	+ve	J1932+1059	B1929+10	+ve	no	-ve	J1932+1500		+ve	no	0
J1932+2220	B1930+22	-ve	no	+ve	J1934+2352		-ve	no	+ve	J1935+2025I		-ve	no	-ve
J1935+2025M		-ve	no	+ve	J1938+0650		-ve	no	+ve	J1938+2010		-ve	no	+ve
J1940+2245		+ve	no	+ve	J1940+2337		+ve	no	+ve	J1941+0121		+ve	no	-ve
J1943-1237	B1940-12	+ve	no	+ve	J1944+1755	B1942+17	-ve	no	-ve	J1946-1312		-ve	no	0
J1949-2524	B1946-25	-ve	no	+ve	J1951+1123		+ve	no	+ve	J1956+0838		+ve	no	-ve
J2002+1637		+ve	no	+ve	J2005-0020		+ve	no	0	J2007+0910		-ve	no	+ve
J2017+2043		+ve	yes	-ve	J2038-3816		-ve	no	0	J2043+2740		+ve	no	+ve
J2048-1616	B2045-16	+ve	no	0	J2108-3429		+ve	yes	0	J2111+2106		+ve	yes	+ve
J2124+1407	B2122+13	-ve	no	0	J2127-6648	B2123-67	-ve	no	0	J2139+2242		-ve	no	0
J2155-3118	B2152-31	+ve	yes	0	J2215+1538		-ve	no	-ve	J2234+2114		-ve	yes	-ve
J2248-0101		+ve	no	0	J2324-6054	B2321-61	+ve	no	0	J2346-0609		+ve	no	0

Table A2. Pulsars classified as flat. The sign of β is given in column 3. Column 4 indicates whether $V > L$ in more than 5 phase bins across the profile. Interpulse pulsars are denoted with an M (main pulse) or I (interpulse) suffix.

JNAME	BNAME	β	V_h								
J0108-1431		-ve	no	J0448-2749		+ve	yes	J0631+0646	-ve	no	
J0934-4154		+ve	no	J1016-5819		-ve	no	J1047-3032	+ve	no	
J1047-6709		+ve	no	J1052-5954		+ve	no	J1054-5943	-ve	no	
J1056-6258	B1054-62	+ve	no	J1119-6127		+ve	no	J1137-6700	-ve	no	
J1154-6250		+ve	no	J1210-6550		+ve	no	J1232-4742	-ve	no	
J1249-6507		-ve	no	J1301-6305		-ve	no	J1339-4712	-ve	yes	
J1347-5947		+ve	no	J1355-6206		+ve	no	J1406-5806	-ve	no	
J1424-5822		+ve	yes	J1452-6036		-ve	no	J1509-6015	-ve	no	
J1511-5414		-ve	no	J1513-5908	B1509-58	-ve	no	J1524-5625	-ve	no	
J1531-5610		+ve	no	J1551-4424		+ve	no	J1603-2531	+ve	no	
J1627-5547		-ve	no	J1638-4417		+ve	no	J1643-4505	+ve	yes	
J1649-4349		-ve	no	J1650-4921		-ve	no	J1652-1400	-ve	no	
J1658-4958		+ve	no	J1701-3130		-ve	no	J1709-4429	B1706-44	-ve	no
J1715-3903		+ve	no	J1718-4539		-ve	no	J1739-3951	-ve	no	
J1740-3052		-ve	no	J1742-4616		-ve	no	J1811+0702	-ve	no	
J1813+1822		-ve	no	J1827-0934		-ve	no	J1832-0644	-ve	no	
J1833-1034		-ve	no	J1836-1324		+ve	no	J1839-0402	-ve	no	
J1842+1332		-ve	no	J1843-0510		+ve	no	J1851+0418	B1848+04	-ve	no
J1856+0113	B1853+01	-ve	no	J1901+0355		+ve	no	J1904+0004	-ve	yes	
J1904+0800		-ve	no	J1904-0150		+ve	no	J1906+0649	-ve	no	
J1907+0345		-ve	no	J1912+1036	B1910+10	+ve	no	J1913+0832M	-ve	no	
J1913+0904		-ve	no	J1913+1000		-ve	no	J1924+1639	+ve	no	
J1928+1443		+ve	no	J1929+2121		+ve	no	J1935+1159	-ve	no	
J1946+1805	B1944+17	-ve	no	J2307+2225		+ve	yes				

Table A3. Pulsars classified as non-RVM. Interpulse pulsars are denoted with an M (main pulse) or I (interpulse) suffix.

JNAME	BNAME								
J0034-0721	B0031-07	J0152-1637	B0149-16	J0206-4028	B0203-40	J0211-8159		J0255-5304	B0254-53
J0302+2252		J0401-7608	B0403-76	J0421-0345		J0450-1248	B0447-12	J0517+2212	
J0520-2553		J0525+1115	B0523+11	J0529-6652	B0529-66	J0533+0402		J0540-7125	
J0601-0527	B0559-05	J0621+0336		J0624-0424	B0621-04	J0629+2415	B0626+24	J0630-0046	
J0647+0913		J0656-2228		J0719-2545		J0725-1635		J0726-2612	
J0733-2345		J0738-4042	B0736-40	J0746-4529		J0749-4247		J0758-1528	B0756-15
J0807-5421		J0809-4753	B0808-47	J0818-3232		J0820-1350	B0818-13	J0823+0159	B0820+02
J0835-3707		J0837+0610	B0834+06	J0837-4135	B0835-41	J0840-5332	B0839-53	J0846-3533	B0844-35
J0855-3331	B0853-33	J0902-6325	B0901-63	J0905-51271		J0908-1739	B0906-17	J0919-6040	
J0922-4949		J0924-5302	B0922-52	J0934-5249	B0932-52	J0941-5244		J0942-5552	B0940-55
J0944-1354	B0942-13	J0949-6902		J0953+0755	B0950+08	J0955-5304	B0953-52	J1001-5507	B0959-54
J1001-5559		J1003-4747	B1001-47	J1012-5857	B1011-58	J1017-5621	B1015-56	J1018-1642	B1016-16
J1034-3224		J1035-6345		J1036-4926		J1036-6559		J1043-6116	
J1046-5813	B1044-57	J1057-5226I	B1055-52I	J1058-5957		J1059-5742	B1056-57	J1112-6613	B1110-65
J1112-6926	B1110-69	J1121-5444	B1119-54	J1123-4844		J1123-6651		J1126-6054M	B1124-60M
J1132-5627		J1133-6250	B1131-62	J1136+1551	B1133+16	J1136-5525	B1133-55	J1141-3322	
J1142-6230		J1144-6217		J1156-5707		J1157-6224	B1154-62	J1159-7910	
J1202-5820	B1159-58	J1210-5559		J1224-6407	B1221-63	J1225-5556		J1225-6035	
J1225-6408	B1222-63	J1231-4609		J1235-6354		J1237-6725		J1239+2453	B1237+25
J1239-6832	B1236-68	J1240-4124	B1237-41	J1243-6423	B1240-64	J1244-5053		J1246+2253	
J1248-6444		J1251-7407		J1257-1027	B1254-10	J1259-6741	B1256-67	J1303-6305	
J1305-6455	B1302-64	J1306-6617	B1303-66	J1308-5844		J1312-6400		J1313+0931	
J1319-6056	B1316-60	J1322-6241		J1324-6302		J1326-5859	B1323-58	J1326-6408	B1323-63
J1327-6222	B1323-62	J1328-4921	B1325-49	J1334-5839		J1336-2522		J1338-6204	B1334-61
J1341-6023		J1355-5153	B1352-51	J1355-5925		J1356-5521		J1357-62	B1353-62
J1405-5641		J1410-7404		J1413-6307M	B1409-62M	J1418-3921		J1420-5416	B1417-54
J1423-6953		J1429-5935		J1430-6623	B1426-66	J1440-6344	B1436-63	J1449-5846	
J1453-6413	B1449-64	J1456-6843	B1451-68	J1501-0046		J1507-6640	B1503-66	J1514-4834	B1510-48
J1517-4356		J1518-3952		J1522-5829	B1518-58	J1524-5706		J1525-5417	
J1527-5552	B1523-55	J1528-4109		J1530-6343		J1534-4428		J1534-5334	B1530-53
J1534-5405	B1530-539	J1536-3602		J1539-5626	B1535-56	J1542-5034		J1543+0929	B1541+09
J1543-0620	B1540-06	J1544-5308	B1541-52	J1547-5750		J1551-6214		J1555-3134	B1552-31
J1557-4258		J1600-5751	B1556-57	J1602-5100	B1558-50	J1603-2712	B1600-27	J1604-4909	B1600-49
J1604-7203		J1607-0032	B1604-00	J1609-4616		J1611-5209M	B1607-52M	J1612+2008	
J1612-5805		J1613-4714	B1609-47	J1615-5537	B1611-55	J1617-4608		J1618-4723	
J1621-5039		J1622-4332		J1623-0908	B1620-09	J1624-4411		J1625-4048	
J1626-6621		J1627-5936		J1632-4621		J1635-5954	B1630-59	J1637-4553	B1634-45
J1638-3815		J1638-5226		J1639-4604	B1635-45	J1645-0317	B1642-03	J1646-6831	B1641-68
J1648-3256		J1649-3805		J1649-3935		J1650-1654		J1651-1709	B1648-17
J1651-4246	B1648-42	J1651-5222	B1647-52	J1654-3710		J1655-3048		J1659-1305	B1657-13
J1700-4939		J1703-4851		J1705-1906I	B1702-19I	J1705-1906M	B1702-19M	J1705-3423	
J1707-4729		J1711-5350	B1707-53	J1714-1054		J1717-5800		J1720+2150	
J1731-4744	B1727-47	J1735-0724	B1732-07	J1738-3211	B1735-32	J1739+0612		J1739-1313	
J1739-2903M	B1736-29M	J1741-3927	B1737-39	J1743-1351	B1740-13	J1744-1610		J1745-0129	
J1745-3040	B1742-30	J1750-3157	B1747-31	J1751-4657	B1747-46	J1752-2806	B1749-28	J1754-3510	
J1755-0903M		J1757-2421	B1754-24	J1801-0357	B1758-03	J1803-3329		J1805+0306	B1802+03
J1805-0619		J1806+1023		J1807-0847	B1804-08	J1807-2715	B1804-27	J1808-1020	
J1809-0119		J1809-0743		J1811-0154		J1811-4930		J1812-1718	B1809-173
J1812-3039		J1814-0521		J1817-3837		J1818-0151		J1820-0427	B1818-04
J1820-0509		J1820-1818	B1817-18	J1821+1715		J1822+0705		J1822-4209	
J1823+0550	B1821+05	J1824-1945	B1821-19	J1825+0004	B1822+00	J1825-0935	B1822-09	J1826-1131	B1823-11
J1827-0750		J1828-0611		J1829-1751	B1826-17	J1832-0827	B1829-08	J1833-0338	B1831-03
J1833-0827	B1830-08	J1834-0031		J1834-1202		J1836-0436	B1834-04	J1836-1008	B1834-10
J1837-0653	B1834-06	J1838+1523		J1838+1650		J1839-0905		J1840-0815	
J1841-0157		J1841-0425	B1838-04	J1843-0459		J1843-1507		J1844+1454	B1842+14

Table A3. Pulsars classified as non-RVM (continued).

JNAME	BNAME								
J1844-0433	B1841-04	J1845+0623		J1845-0743		J1847-0402	B1844-04	J1848+1516	
J1848-0023		J1848-0123	B1845-01	J1848-1150		J1849-0636	B1846-06	J1852-0118	
J1852-2610		J1853-0004		J1857+0212	B1855+02	J1859+1526		J1900-2600	B1857-26
J1900-7951	B1851-79	J1901+0156	B1859+01	J1901+0331	B1859+03	J1901-0906		J1902+0556	B1900+05
J1903+0135	B1900+01	J1904-1224		J1905-0056	B1902-01	J1906+0641	B1904+06	J1907-1532	
J1909+0007	B1907+00	J1909+0254	B1907+02	J1909+1102	B1907+10	J1909+1859		J1910+0358	B1907+03
J1910+0714		J1910+1231	B1907+12	J1910-0309	B1907-03	J1913+1400	B1911+13	J1913-0440	B1911-04
J1915+0227		J1915+1009	B1913+10	J1916+0951	B1914+09	J1916-2939		J1919+0021	B1917+00
J1919+0134		J1921+1948	B1918+19	J1921+2003	B1919+20	J1921+2153	B1919+21	J1923+1706	B1921+17
J1926+0431	B1923+04	J1929+1955		J1930+1316	B1927+13	J1930-1852		J1932-3655	
J1933+1304	B1930+13	J1935+1616	B1933+16	J1936+1536	B1933+15	J1938+2213		J1941+1341	
J1941-2602	B1937-26	J1943+0609		J1945-0040	B1942-00	J1946+2244	B1944+22	J1946-2913	B1943-29
J1947+0915		J1949+2306		J1952+1410	B1949+14	J2006-0807	B2003-08	J2037+1942	B2034+19
J2045+0912		J2046+1540	B2044+15	J2046-0421	B2043-04	J2053-7200	B2048-72	J2116+1414	B2113+14
J2136-1606		J2144-3933		J2154-2812		J2253+1516		J2317+2149	B2315+21
J2330-2005	B2327-20								

Table A4. Pulsars for which an RVM fit was not attempted. Interpulse pulsars are denoted with an M (main pulse) or I (interpulse) suffix.

PSR						
J0038–2501	J0045–7319	J0111–7131	J0113–7220	J0131–7310		
J0133–6957	J0137+1654	J0418–4154	J0449–7031	J0455–6951	B0456–69	
J0456–7031	J0457–6337	J0502–6617	B0502–66	J0511–6508		
J0519–6932	J0522–6847	J0532–6639	J0540–6919	B0540–69	J0543–6851	
J0623+0340	J0628+0909	J0633+1746	J0636–4549	J0652–0142		
J0656–5449	J0658+0022	J0804–3647	J0808–3937	J0815+0939		
J0820–3826	J0820–4114	B0818–41	J0828–3417	B0826–34	J0834–4159	J0836–4233
J0927+2345	J0930–2301	J0943+2253	J1006–6311	J1012–5830		
J1019–5749	J1020–6026	J1021–5601	J1028–5819	J1031–6117		
J1048–5838	J1054–5946	J1055–6236	J1056–5709	J1057–4754		
J1106–6438	J1107–5907	J1112–6103	J1116–2444	J1124–5916		
J1124–6421	J1126–6054I	B1124–60I	J1130–5925	J1138–6207		
J1143–5158	J1156–5909	J1201–6306	J1214–5830	J1216–6223		
J1233–6312	J1233–6344	J1234–3630	J1243–5735	J1244–6359		
J1248–6344	J1255–6131	J1306–6242	J1309–6526	J1316–6232		
J1317–5759	J1317–6302	J1320–3512	J1321–5922	J1327–6400		
J1332–3032	J1333–4449	J1337–6306	J1341–6220	B1338–62	J1346–4918	
J1349–6130	J1359–6038	B1356–60	J1406–6121	J1407–6048		
J1409–6953	J1410–6132	J1412–6145	J1413–6141	J1413–6222		
J1425–5723	J1425–5759	J1433–6038	J1434–6006	J1437–6146		
J1444–6026	J1457–5902	J1503+2111	J1504–5621	J1509–5850		
J1511–5835	J1512–5759	B1508–57	J1514–5925	J1515–5720		
J1518–5415	J1519–5734	J1525–5523	J1525–5605	J1535–5450		
J1536–5907	J1538–5438	J1538–5551	J1538–5621	J1538–5750		
J1539–5521	J1543–5459	J1546–5302	J1547–5839	J1548–4821		
J1548–5607	J1549–4848M	J1549–5722	J1550–5418	J1551–5310		
J1555–0515	J1600–5044	B1557–50	J1604–4718	J1607–6449		
J1610–5006	J1611–5209I	B1607–52I	J1613–5211	J1614–5048	B1610–50	
J1617–5055	J1620–5414	J1621–5243	J1623–0841	J1625–4904		
J1625–4913	J1627+1419	J1627–4706	J1630–4719	J1630–4733	B1626–47	
J1632–4757	J1632–4818	J1633–4453	B1630–44	J1633–5015	B1629–50	J1634–5107
J1635+2332	J1636–4440	J1637–4450	J1638–4608	J1638–4725		J1638–4725
J1640–4648	J1640–4715	B1636–47	J1643–4550	J1644–4657		J1644–4657
J1645+1012	J1647–3607	J1648–4611	J1649–4653	J1650–4126		J1650–4126
J1650–4341	J1650–4502	J1653–4249	J1657–4432	J1659–4439		J1659–4439
J1700–4012	J1700–4422	J1701–4533	B1657–45	J1702–4128		J1702–4306
J1705–4331	J1706–6118	J1707–4053	B1703–40	J1708–3641		J1709–3841
J1710–4148	J1711–4322	J1715–3859	J1716–4111	J1717–3425		B1714–34
J1717–3737	J1717–4054	B1713–40	J1719–4006	B1715–40	J1720–3659	J1721–3532
J1722–3632	B1718–36	J1724–3149	J1725–0732	J1725–3546		J1726–3635
J1726–4006	J1730–3350	B1727–33	J1731–3123	J1732–3131		J1732–4156
J1734–2415	J1734–3058	J1735–3258	J1738–2647	J1738–2736		J1738–2736
J1739–3131	B1736–31	J1740–3327	J1741–2054	J1741–2945		J1743–3153
J1744–3922	J1744–5337	J1746–2849	J1746–2856	J1747–2809		J1747–2809
J1747–2958	J1748–2021A	B1745–20A	J1749–2629	J1749–5417		J1752+2359
J1755–0903I	J1755–2025	J1755–2521	J1755–2550	J1755–26		J1755–26
J1756–2225	J1758–1931	J1758–2540	J1759–2307	J1759–2549		J1759–2549
J1801–2154	J1801–2304	B1758–23	J1801–2451	B1757–24	J1802–1745	J1802–2426
J1803–1920	J1805–2032	J1806–1618	J1806–2125	J1807+0756		J1807+0756
J1808–1517	J1810–1441	J1810–1820	J1811–1736	J1811–2439		J1811–2439
J1812+0226	B1810+02	J1812–1733	B1809–176	J1814–1744		J1815–1738
J1816–0755I	J1816–1729	B1813–17	J1816–5643	J1818–1422	B1815–14	J1819–1114
J1819–1510	J1819–1717	J1820–1346	B1817–13	J1820–1529		J1821–0256
J1821–1432	J1822+1120	J1822–1400	B1820–14	J1824–0132		J1824–1118
J1824–1159	J1824–1350	J1824–1423	J1825–1446	B1822–14	J1826–1419	B1821–11

Table A4. Pulsars for which an RVM fit was not attempted (continued)

JNAME	BNAME						
J1827-0958	B1824-10	J1828-1007	J1828-1057		J1828-1101	J1828-2119	
J1829+0000		J1829-0734	J1832-1021	B1829-10	J1833-0559	J1834-0010	B1831-00
J1834-0426	B1831-04	J1834-0731	J1834-0742		J1835-0643	B1832-06	J1835-09242
J1837-0559		J1837-0604	J1837-0822		J1838-0453		J1838-0549
J1839-0141		J1839-0223	J1839-0321		J1839-0332		J1839-0459
J1839-0643		J1840-0559	J1840-0643		J1840-1419		J1841-0500
J1841-7845		J1842-0153	J1842-0415		J1842-0800		J1843+2024
J1843-0137		J1843-0355	J1843-0702M		J1843-0744		J1844-0030
J1844-0244	B1842-02	J1844-0302	J1844-0452		J1844-0538	B1841-05	J1845-0826
J1846-0257		J1846-0749	J1847-0443		J1848+0351		J1848+0647
J1848+0826		J1848-0601	J1848-1243		J1849+0409I		J1850+0423
J1850-0006		J1850-0026	J1851+0233		J1851-0029		J1851-0114
J1852+0008		J1852+0013	J1852-0127		J1853+0011		J1853+0505
J1853+0545		J1854+0306	J1855+0205		J1855+0527		J1855+0700
J1856+0102		J1856+0245	J1857+0143		J1857+0300		J1857+0526
J1857+0809		J1858+0319	J1858+0346		J1859+0601		J1859+0603
J1900+0438		J1900+0634	J1901+0459		J1901+0511		J1902-1036
J1903+0601		J1903+0654	J1903-0258		J1904+0738		J1905+0600
J1905+0902		J1906+0414	J1906+0509		J1906+0746		J1906+0912
J1906+1854		J1907+0255	J1907+0602		J1907+0731		J1907+0859
J1907+1247	B1904+12	J1908+0734	J1908+0833		J1908+0839		J1908+0909
J1908+0916	B1906+09	J1908+2351	J1909+0641		J1909+0912		J1909+1148
J1910+0225		J1910+0517	J1913+0657		J1913+0832I		J1913+1011
J1913+1050		J1913+1145	J1913+1330		J1914+0631		J1915+0838
J1915+1410		J1916+0844	J1916+1030	B1913+105	J1916+1225		J1917+1737
J1918+1541I		J1919+1314	J1919+1645		J1921+1544		J1922+1131
J1926+0737		J1926+1928	B1924+19	J1926-1314	J1927+0911		J1927+1856
J1928+1923		J1929+1357		J1929+1844	B1926+18		J1931+1952
J1933+0758		J1935+1745	B1933+17	J1941+1026	J1942+1743	B1939+17	J1945+1834
J1947+1957		J1948+2333		J1953+1149	J1954+1021		J1954+2407
J2013-0649		J2027+2146	B2025+21	J2040+1657	J2048+2255		J2051+1248
J2053+1718		J2151+2315		J2205+1444	J2243+1518		